Morphology-Controllable Synthesis and Characterization of Single-Crystal Molybdenum Trioxide

Tian Xia,[†,‡] Qin Li,[†,‡] Xiangdong Liu,[†,‡] Jian Meng,[†] and Xueqiang Cao*[,†]

Key Laboratory of Rare Earth Chemistry and Physics, Changchun Institute of Applied Chemistry, Chinese Academy of Sciences, Changchun 130022, Jilin, People's Republic of China, and Graduate School of the Chinese Academy of Sciences, Beijing 100049, People's Republic of China

Received: October 17, 2005; In Final Form: December 9, 2005

Molybdenum trioxide nanobelts and prism-like particles with good crystallinity and high surface areas have been prepared by a facile hydrothermal method, and the morphology could be controlled by using different inorganic salts, such as KNO_3, $Ca(NO_3)_2$, $La(NO_3)_3$, etc. The possible growth mechanism of molybdenum trioxide prism-like particles is discussed on the basis of the presence of H^+ and the modification of metal cations. The as-prepared nanomaterials are characterized by means of powder X-ray diffraction (PXRD), field-emission scanning electron microscopy (FE-SEM), transmission electron microscopy (TEM), high-resolution TEM (HRTEM), Fourier transformation infrared spectroscopy (FT-IR), X-ray photoelectron spectroscopy (XPS), and ultraviolet and visible spectroscopy (UV−vis). TEM and HRTEM micrographs show that the molybdenum trioxide nanobelts and prism-like particles have a relatively high degree of crystallinity and uniformity. BET specific surface areas of the as-prepared molybdenum trioxide nanocrystals are 67−79 $m^2\ g^{-1}$. XPS analysis indicates that the hexavalent molybdenum is predominant in the nanocrystals. UV−vis spectra reveal that the direct band gap energy of the annealed molybdenum trioxide prism-like particles shows a pronounced blue shift compared to that of bulk MoO_3 powder. Interestingly, molybdenum trioxide nanobelts exhibit a red shift under this condition.

Introduction

Over the past decade, nanometer science and technology have been one of the critical compositions in materials science. Recent efforts have been focused on not only the development of new synthesis routes for novel nanocrystals,[1] but also the preparation of functional material with special morphology, and the morphology-controllable synthesis.[2] The effect of dimensionality and geometry on material properties has been extensively studied on the nanomaterials. In particular, one-dimensional nanosized compounds including nanotubes,[3−8] nanorods,[9−12] nanowires,[13−18] and nanoribbons and nanobelts[19−25] are likely to be a model materials family for systematic understanding in the electrical, magnetic, optical, and ionic transport properties.

Since the discovery of the carbon nanotube with novel properties,[3] many wirelike nanomaterials have been fabricated successfully in recent years because of their great potential for addressing some basic issues about dimensionality and space-confined effect as well as technological applications. Another group of distinctly different semiconducting oxide nanostructures corresponding to belt-like morphology was reported.[19] These oxides with the nanoribbon's or nanobelt's morphology cover cations with different valence states and materials with different crystallographic structures. This will be an exciting and potential new field for nanotechonology.

Molybdenum trioxide is an interesting electrochromic and photochromic material,[26,27] a gas sensor device,[28] and one of the most widely used catalysts.[29−31] In addition, it is noted that molybdenum trioxide is also a good precursor for synthesizing other important compounds, such as MoO_2, MoS_2, $MoSe_2$, Mo, etc.[32−37] Many morphologies of molybdenum trioxide crystals based on different procedures and synthesis techniques are now prepared, such as molybdenum trioxide nanorods,[38] nanotubes,[37,39] hollow MoO_3 nanospheres and mesostructured toroids,[40,41] and molybdenum trioxide fibers or nanobelts.[42−44] Li and co-workers reported a hydrothermal method for the growth of MoO_3 nanobelts using Na_2MoO_4 as the starting material, and they obtained large-scale single-crystal MoO_3 nanobelts.[43] Some fundamental characteristics of one-dimensional MoO_3 nanostructures were obtained. However, there remains much interest in morphology-controllable synthesis and novel properties. In this paper, a novel, facile hydrothermal process leading to MoO_3 nanobelts and prism-like particles has been developed, and the morphology of particles could be controlled in the presence of different inorganic salts. The movitations of this research are to develop a hydrothermal method to prepare molybdenum trioxide nanomaterials, to investigate physical and chemical properties of one-dimensional nanostructures, and to understand the formation mechanism of nanocrystals. The molybdenum trioxide samples were characterized by the techniques of powder X-ray diffraction (PXRD), X-ray photoelectron spectroscopy (XPS), transmission electron microscopy (TEM) and scanning electron microscopy (SEM), nitrogen adsorption, Fourier transformation infrared spectroscopy (FT-IR), and ultraviolet and visible spectroscopy (UV−vis). In this work, the facile morphology-controllable synthesis, shape-dependent UV adsorption, and increased and decreased band gap are presented.

Experimental Section

1. Synthesis. The syntheses of MoO_3 nanocrystals were carried out by a hydrothermal technique. $(NH_4)_6Mo_7O_{24}\cdot 4H_2O$

* Corresponding author. E-mail: xcao@ciac.jl.cn.
[†] Changchun Institute of Applied Chemistry, Chinese Academy of Sciences.
[‡] Graduate School of the Chinese Academy of Sciences.

10.1021/jp055945n CCC: $33.50
Published on Web 01/19/2006

(A. R. grade, ≥99.0%) was used as the source of molybdenum. In a typical procedure, 1 mmol of $(NH_4)_6Mo_7O_{24}\cdot 4H_2O$ was dissolved into 30 mL of distilled water and 10 mmol of KNO_3 and $NaNO_3$ (A. R. grade, ≥99.0%), 5 mmol of $Ca(NO_3)_2$ (A. R. grade, ≥99.0%), and 3 mmol of $La(NO_3)_3$ (A. R. grade, ≥99.9%) were dissolved in 20 mL of distilled water, respectively. Then $(NH_4)_6Mo_7O_{24}$ solution was slowly added into nitrates solution under magnetic stirring to form a homogeneous aqueous solution at room temperature. The pH value was adjusted to 1−3 with HNO_3 (1 mol L^{-1}) solution. The as-obtained solution was transferred into a 100 mL Teflon-lined stainless autoclave, sealed, and heated at 180 °C for 24−36 h in a digital type temperature controlled oven, then allowed to cool to room temperature naturally. The white products were recovered by filtration, washed with deionized water several times, and dried overnight in a vacuum at 60 °C. After drying, the product was annealed at 500 °C in oxygen for 2 h.

2. Characterization Methods. The powder X-ray diffraction (PXRD) patterns were recorded on a Rigaku D/MAX-2500 diffractometer with Cu Kα radiation ($\lambda = 0.15406$ nm) and a scanning rate of 2 deg min^{-1}. The operation voltage and current were maintained at 40 kV and 200 mA, respectively. The lattice parameters were calculated by the Rietveld analysis[45] of the PXRD data with the Material Studio software.

The transmission electron micrograph (TEM) and the selected area electron diffraction (SAED) were taken with a JEOL-JEM-2010 operating at 200 kV (JEOL, Japan). Samples for TEM were prepared by dropping a diluted suspension of the sample powders onto a standard carbon-coated (20−30 nm) Formvar film on a copper grid (230 mesh). The field-emission scanning electron microscopy (FE-SEM, XL-30, Philips) equipped with energy-dispersive X-ray fluorescence analysis (EDXA) was used to investigate the morphology of samples. For SEM observation, the product was pasted on the silicon substrate.

Fourier transformation infrared spectroscopy (FT-IR) was acquired with a Nicolet FT-IR SX520 spectrometer. FT-IR spectra on the powders were measured on pellets prepared by mixing the powders with KBr with a sample:KBr volume ratio of about 1:50.

X-ray photoelectron spectroscopy (XPS) experiments were conducted with a VG ESCALAB MK Π spectrometer (VG Scientific, UK) in an ion-pumped chamber (evacuated to 2×10^{-9} Torr), and employing a monochromatic Mg Kα X-ray source ($h\nu = 1253.6$ eV). The binding energy (BE) for the samples was calibrated by setting the measured BE of C1s to 284.6 eV.

The UV−visible absorption spectroscopic measurements were performed on a HITACHI U-4100 spectrophotometer, using a quartz cell with width of 1 cm. The as-synthesized powder was dispersed in ethanol with a concentration of about 10^{-4} mol L^{-1} and then sonicated at room temperature for 30 min, and a colloidal solution was thus obtained; pure ethanol was used as a blank. The optical absorption coefficient α was calculated according to the following equation:[46,47]

$$\alpha = [(2.303 \times 10^3)A\rho]/lc$$

where A is the absorbance of a sample, ρ is the real density of MoO_3 (4.71 g cm^{-3}), l is the path length, and c is the concentration of the suspensions.

The Brunauer−Emmett−Teller (BET) surface area was measured on a Quantachrome NOVA 1000 Ver 6.11 system at 77.4 K. All samples were first degassed in a vacuum at 200 °C for 2 h before analysis. The BET-specific area was calculated from the nitrogen adsorption data in the relative pressure range from 0.05 to 0.3. The total volume was estimated from the amount adsorbed at a relative pressure of about 0.99.

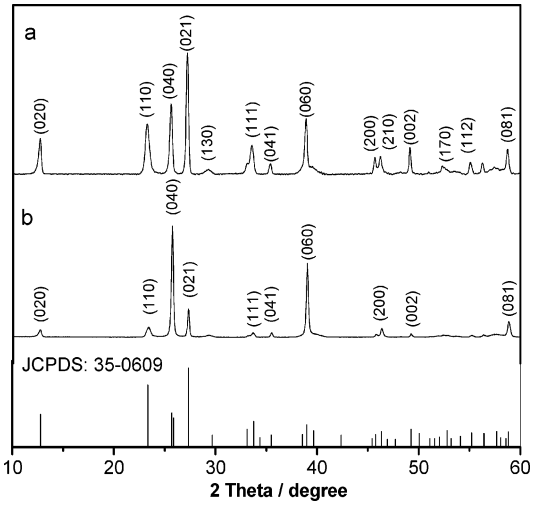

Figure 1. PXRD patterns for as-prepared samples: (a) nanobelts and (b) prism-like particles.

TABLE 1: The Lattice Parameters and BET Specific Surface Areas (S_{BET}) of the As-Prepared and Annealed Samples

morphology	a (Å)	b (Å)	c (Å)	cell vol, V (Å^3)	S_{BET},[a] $m^2\,g^{-1}$	S_{BET},[b] $m^2\,g^{-1}$
belts	3.965(2)	13.875(5)	3.703(1)	203.69	66.9	69.3
prism-like	3.959(1)	13.848(1)	3.698(1)	202.73	78.9	82.1

[a] BET surface areas calculated from the linear part of the BET plot ($P/P_0 = 0.05-0.3$). [b] Annealed at 500 °C in oxygen for 2 h.

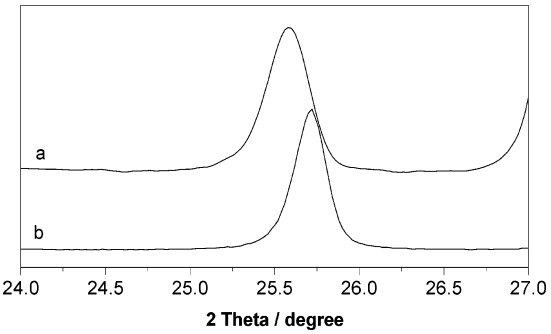

Figure 2. PXRD patterns ($2\Theta = 24-27°$) for as-prepared samples: (a) nanobelts and (b) prism-like particles.

Results and Discussion

1. Characteristics of Molybdenum Trioxide Nanocrystals. Figure 1 shows the PXRD patterns of the as-prepared molybdenum trioxide nanobelts and prism-like particles. All the diffraction peaks can be indexed as an orthorhombic-phase MoO_3 (JCPDS 35-0609, $a = 0.3963$ nm, $b = 1.3856$ nm, $c = 0.3697$ nm, space group *Pbnm*). The lattice parameters calculated from this pattern are summarized in Table 1. An observation of the reflection peak (040) at 25.5° (Figure 2) reveals that there is a downshift from prism-like particles to nanobelts with a corresponding increase in the unit cell volumes (Table 1).

Molybdenum trioxide nanobelts and prism-like particles were prepared by mixing ammonium heptamolybdate tetrahydrate and nitrates (KNO_3 and $La(NO_3)_3$). The optimal reaction conditions for the formation of MoO_3 nanobelts and prism-like samples are summarized in Table 2. The morphology of obtained MoO_3 nanocrystals was examined by FE-SEM and TEM. Representa-

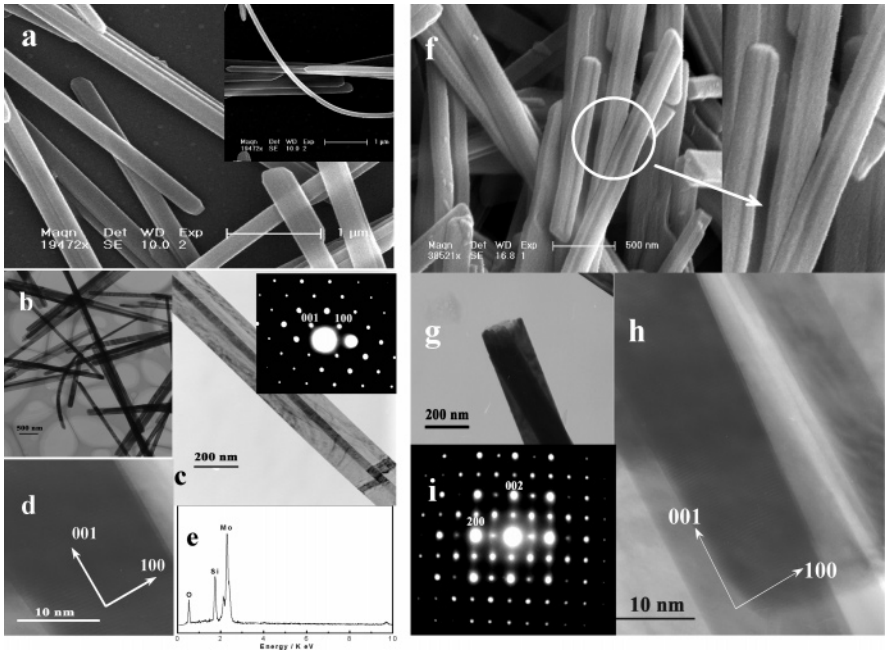

Figure 3. (a) SEM images of as-prepared MoO_3 nanobelts, (b and c) MoO_3 nanobelt TEM images and its selected area electron diffraction pattern (inset), (d) HRTEM image of an individual MoO_3 nanobelt, (e) EDX of nanobelts showing the ratio of Mo:O ≈ 3:1, (f) SEM and (g) TEM images of as-prepared MoO_3 prism-like particles, (h) HRTEM image of an individual prism-like particle, and (i) selected area electron diffraction image of MoO_3 prism-like particles.

TABLE 2: Summary of Experimental Conditions

morphology	nitrate	nitrate concn, mM	pH value	reaction time (h)
belts	KNO_3	10	1	24
belts	$NaNO_3$	10	1	24
prism-like	$La(NO_3)_3$	3	2	36
rods	$Ca(NO_3)_2$	5	2	36
rods			1	36

tive SEM and TEM micrographs of MoO_3 nanobelts are shown in Figure 3a−d. These figures reveal uniform nanobelts with a width of 200−300 nm and a thickness of 50−100 nm, and lengths of several tens of micrometers. An HRTEM image of an individual nanobelt (Figure 3c) provides that clearly resolved bending contours indicate a high degree of crystallinity within the domains of the nanostructured oxide. The selected area electron diffraction (SAED) pattern (inset of Figure 3c) recorded perpendicular to the growth axis of the single nanobelt could be attributed to the [010] zone axis diffraction of orthorhombic MoO_3, and suggests that nanobelts grew along the [001] direction. The results indicate that the samples are single-crystalline nanobelts with high crystallinity. The energy-dispersive X-ray spectroscopy analysis (EDXA) confirms that the nanobelts are composed of Mo and O in a ratio of about 1:3 (Figure 3e). Furthermore, no traces of potassium or lanthanum are detected in the final MoO_3 products.

Representative SEM and TEM images of MoO_3 prism-like particles are shown in Figure 3f−i. The MoO_3 prism-like particles are formed with widths of 200−300 nm, lengths ranging from 1 to 3 μm, and aspect ratios of 4−10. The enlarged image of the SEM micrograph further shows the edges of prisms. Moreover, each prism-like particle shows a polygonal cross section with a thickness of about 50−100 nm. The HRTEM and SAED results are similar to those of MoO_3 nanobelts. The above-mentioned investigations reveal that the morphology of MoO_3 nanocrystals can be controlled with the addition of common nitrates.

The growth mechanism of one-dimensional MoO_3 nanocrystals has been investigated by the groups of Lou[38] and Patzke.[44] Although we have not determined the exact growth mechanism of MoO_3 prism-like particles, the growth process of the prism-like particles through the hydrothermal procedure was discussed according to the early reports and this experimental condition. In our experiment, the only difference between the synthesis of belt-shaped and prism-like MoO_3 nanocrystals is the addition of KNO_3 and $La(NO_3)_3$ into the molybdenum precursor separately. The results from the samples with HNO_3 suggest that the acidity in the molybdenum precursor is responsible for the high-yield one-dimensional MoO_3 nanocrystals. The growth process can be understood by electroneutral and dehydration reactions, which is formulated as follows:

$$Mo_7O_{24}^{6-} + 6H^+ + 11H_2O \rightarrow 7MoO_3{\cdot}2H_2O$$

With increasing temperature, $MoO_3{\cdot}2H_2O$ will lose the water as described in the flowing reactions:

$$MoO_3{\cdot}2H_2O \rightarrow \alpha\text{-}MoO_3{\cdot}H_2O + H_2O$$

$$\alpha\text{-}MoO_3{\cdot}H_2O \rightarrow \alpha\text{-}MoO_3 + H_2O$$

The crystal structure of $MoO_3{\cdot}2H_2O$ is monoclinic symmetry and does not display any one-dimensional chain structure.[48] α-$MoO_3{\cdot}H_2O$ exhibits Mo−O−Mo chains running along the [001] direction.[49] Finally, α-MoO_3 has the maximum intensity of one-dimensional growth due to the presence of two different sorts of chains along the *a* and *c* axis, respectively. There is an intrinsic tendency to grow into rodlike nanoparticles due to the anisotropic monoclinic structure of $MoO_3{\cdot}2H_2O$, which is similar to the anisotropic growth of $La(OH)_3$ and $Tb(OH)_3$ under hydrothermal conditions.[50,51] Such a one-dimensional structure usually appears in transition metal oxides.[52,53] Penn and Banfield believe that impetus for the aggregation of nanoparticles is to minimize surface energy.[54] The same mechanism was also identified by Weller's group for the growth of ZnO nanorods

SCHEME 1: Schematic Illustration Showing the Formation Mechanism of MoO_3 Nanobelts and Prism-like Particles[a]

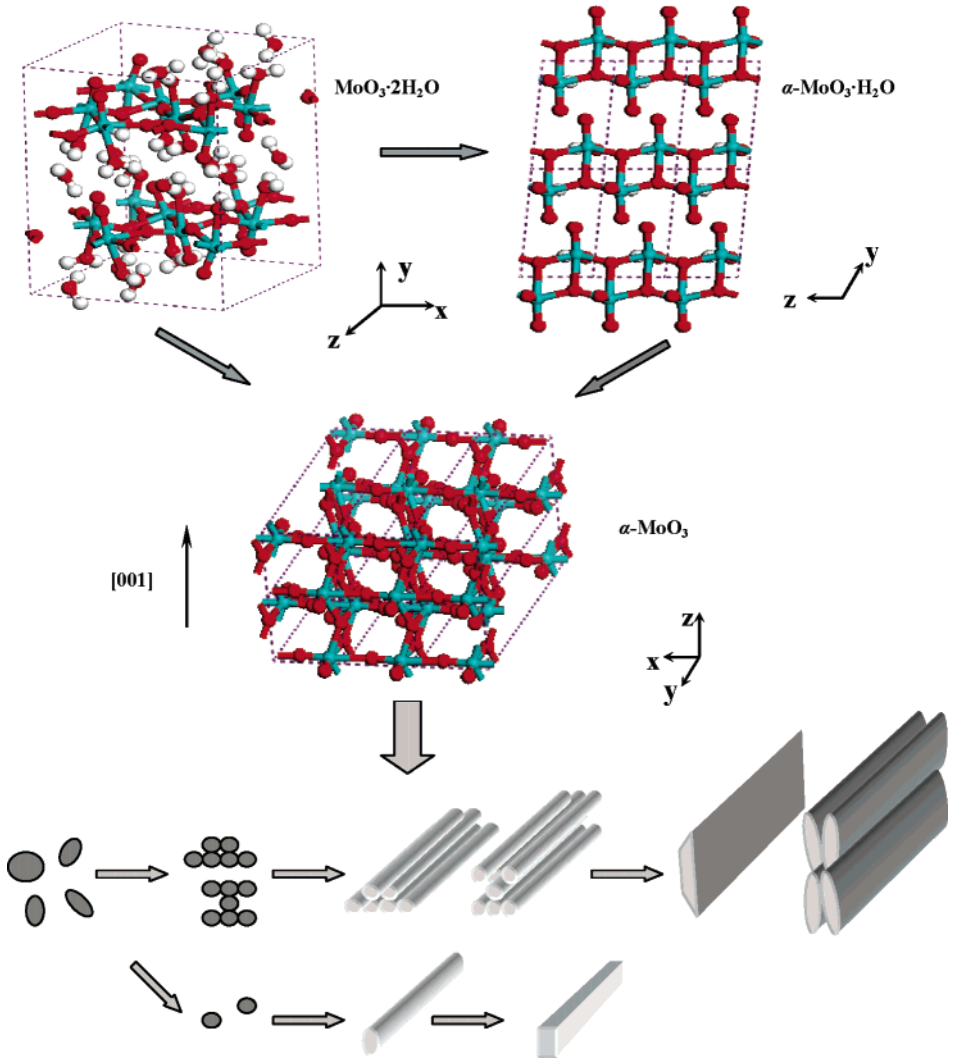

[a] Crystal structures of $MoO_3 \cdot 2H_2O$, α-$MoO_3 \cdot H_2O$, and α-MoO_3 exhibit the gradually increasing tendency toward the formation of a one-dimensional structure.

in a solvothermal system.[53] They found that the nanoparticles served as seeds for the growth of nanorods. In our case, the different metal cations might be responsible for belt-shaped and prism-like particles. The orthorhombic structured MoO_3 has a distinctive layered structure; we propose that K^+ and La^{3+} probably serve as the templates between two MoO_3 monolayers. The La^{3+} has stronger affinity for $Mo_7O_{24}^{6-}$ in comparison with K^+, which results in the aggregation of nanoparticles. These particles act as crystal seeds self-assembled into arrays along the cross-sectional diameter direction, which probably match well and offer a low surface energy in the presence of La^{3+} and NO_3^-. Then the crystal planes along the prism's axial direction grew toward the formation of linear products. The crystal structures of $MoO_3 \cdot 2H_2O$, α-$MoO_3 \cdot H_2O$, and α-MoO_3 and the probable growth process of MoO_3 nanobelts and prism-like particles are illustrated in Scheme 1.

Physicochemical properties of as-prepared and annealed samples are listed in Table 1. The BET surface area of MoO_3 prism-like particles is higher than that of nanobelts. The prism-like structure can be considered as self-assembling of some nanorods or nanobelts. Therefore, the surface area with prism-like structure increases. Interestingly, the surface areas of both belt and prism-like samples increase after anneal. High-temperature treatment initiates the crystallization of compounds and the nanoparticles retain belt and prism-like morphology (Figure S1, Supporting Information). The secondary structure of annealed belt and prisms-like shape can be understood as the agglomeration of each primary nanoparticle, which results in the increment of surface area after anneal. The nitrogen adsorption isotherms for as-prepared and annealed nanobelts and prism-like structures are shown in Figure S2.

Figure 4 typically depicts the XPS spectra of the as-synthesized MoO_3 nanomaterials. Peaks of Mo3d, Mo2p, and O1s can be identified for MoO_3 nanobelts from Figure 4a. No peaks ascribable to N1s and C1s are observed. From Figure 4b and 4c, we can find that two Mo3d binding energy peaks for MoO_3 nanobelts and prism-like particles are consistent with the previous report of Mo (VI)[55] and no apparent Mo^{5+} (V) or Mo^{4+} (IV) is observed, indicating the main valance of molybdenum in these samples is +6. Therefore, the molecular formula of the as-prepared molybdenum oxide nanocrystals should be expressed as $MoO_{3-\delta}$, where δ represents the number of oxygen vacancies.

Figure 5a shows the FT-IR of MoO_3 nanobelts and prism-like particles measured in the 4000−450 cm^{-1} spectral region. It can be seen that all the peaks of the nanobelts and prism-like particles are similar. However, peak B is red-shifted from 877 cm^{-1} (nanoprisms) to 874 cm^{-1} (nanobelts); peak C is red-

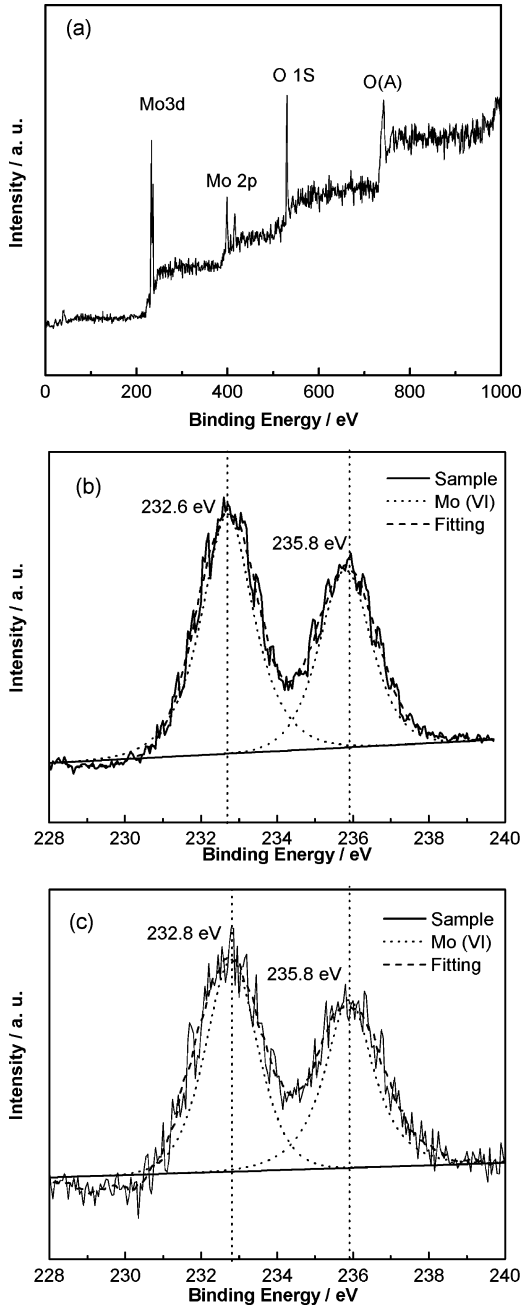

Figure 4. XPS patterns of as-prepared MoO_3 samples: (a) survey spectra of nanobelts, (b) Mo3d spectra of nanobelts, and (c) Mo3d spectra of prism-like particles.

shifted from the 561 cm^{-1} (nanoprisms) to 555 cm^{-1} (nanobelts). The red-shifting may be due to the increment of suspending bonds on the surface of the nanostructures. The FT-IR of as-prepared nanobelts shows three peaks at 555, 874, and 995 cm^{-1}. The peak at 995 cm^{-1} is due to the terminal Mo═O bond, which is an indicator of the layered orthorhombic MoO_3 phase.[56] Absorption at 874 cm^{-1} is attributed to the Mo−O−Mo vibrations of Mo^{6+},[57] which is in good agreement with the XPS analysis. The absorption at 555 cm^{-1} is due to the bending mode vibration of the Mo−O−Mo entity, while the O ion is shared by three Mo ions.[58] The FT-IR spectrum of MoO_3 nanobelts in the 1500−3800 cm^{-1} spectral region is shown in Figure 5b. The broad band at 3390 cm^{-1} is due to O−H stretches of water associated with the powder. The band at 1630 cm^{-1} is ascribed to the bending model of hydroxyl groups of the adsorbed water.

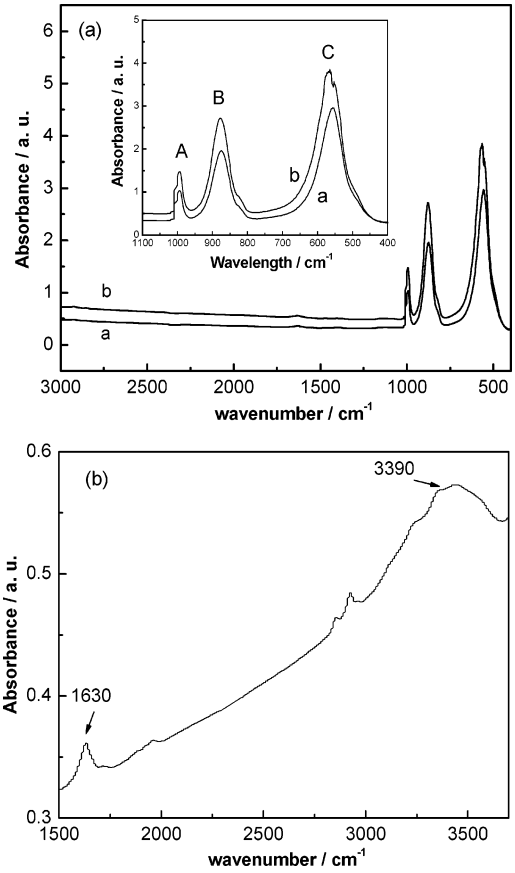

Figure 5. FT-IR spectra for (a) MoO_3 nanobelts (spectrum a) and prism-like particles (spectrum b) and (b) MoO_3 nanobelts in 1500−3800 cm^{-1} spectra region.

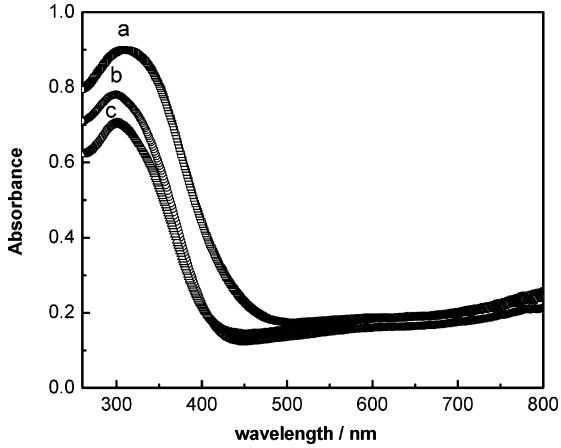

Figure 6. UV spectra for (a) annealed MoO_3 nanobelts, (b) bulk MoO_3 sample, and (c) prism-like particles.

2. UV Absorption Spectra and Band Gap Energies. To reveal the correlation between the band gap energies and morphology of the samples, the UV−vis absorption spectra of annealed MoO_3 nanobelts and prism-like particles are recorded and shown in Figure 6. Both the nanobelts and prism-like particles exhibit a strong adsorption band between 250 and 400 nm in the UV range, which originates from the charge transfer of the Mo−O band in the MoO_6^{6-} octahedron.[59] No absorption was detected above 500 nm in wavelength. A significant blue-shifting of the absorption threshold edge can be observed for the MoO_3 prism-like particles, contrasting with the bulk powder. However, the UV−vis spectrum of nanobelts shows a red-shifting phenomenon in this condition. The plots of $(\alpha h\nu)^2$ vs

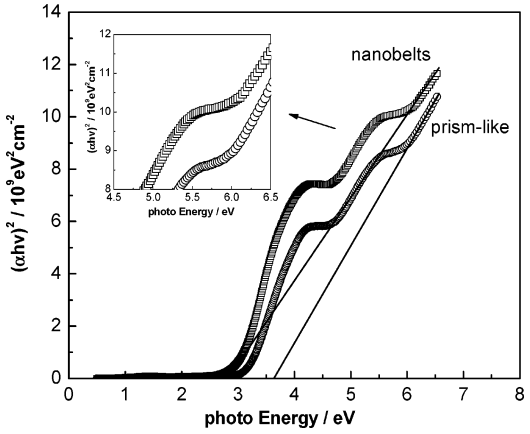

Figure 7. Plots of $(\alpha h\nu)^2$ vs photoenergy for the annealed samples.

photoenergy of annealed MoO_3 nanobelts and prism-like particles are shown in Figure 7. For direct transitions, the absorption coefficient near the absorption edge can be expressed in the following equation:[60]

$$\alpha \propto \frac{\sqrt{h\nu - E_d}}{h\nu}$$

where E_d is the band gap energy for direct transition and $h\nu$ is the photoenergy. From the intersection of the extrapolated linear portion, the E_d values of the MoO_3 nanobelts and prism-like particles can be determined as 2.82 and 3.64 eV, respectively. Compared to the nonoriented polycrystalline MoO_3 ($E_d = 3.05$ eV),[61] MoO_3 prism-like structures and nanobelts show an increase and decrease in E_d by a value exceeding 0.59 and less than 0.23 eV, respectively. Generally, the absorption of molybdenum trioxide in the UV region originates from the charge-transfer transition in the Mo−O band. This absorption is much stronger than the d−d electronic transition in the Mo complex. It was theoretically deduced that the value of blue-shifting resulting from the reduction of particle size is inverse proportional to the square of the size due to the quantum confinement effect.[62]

In a bulk crystal, the properties of the material are independent of the size and are only chemical composition dependent. As the size of a crystal decreases to the nanometer regime, the size of the particle begins to modify the properties of the crystal. Furthermore, depending on the relationship of the radius of the crystal to the Bohr radius of the bulk exciton, $\alpha_B = \epsilon\hbar^2/\mu e^2$, where μ is the exciton-reduced mass and ϵ is the dielectric constant of the semiconductor. The quantum confinement effect can be divided into three regimes: strong confinement, intermediate confinement, and weak confinement regimes, which correspond to $\alpha \ll \alpha_B$, $\alpha \sim \alpha_B$, and $\alpha \gg \alpha_B$, respectively.[63−65] However, the sizes of MoO_3 nanocrystals are not very small with the exception of the thickness (50−100 nm) of nanoparticles. It is unlikely that the quantum size confinement at this length scale is significant enough to cause the blue-shifting. The size confinement effect is clearly insufficient to explain the observed shift pattern. On the basis of the contraction of cell volume for MoO_3 prism-like particles (Table 1), we propose that the blue-shifting is probably attributed to the internal strains. The basic assumption of our model is the presence of nonnegligible internal strains in the nanocrystals. Different growth directions will cause different surface reconstruction, and subsequently lead to internal strains of different magnitudes and directions, which will cause the blue-shifting in phonon wavelengths of low-dimensional nanomaterials.

On the other hand, the red-shifting in the phonon wavelength has also been attributed to the presence of impurities and defects, such as point defects, twins, and stacking faults.[66,67] These defects which usually appear in substoichiometric transition metal oxides are also likely to be responsible for additional vibrational modes of low-dimensional nanomaterial. Dai et al. also proposed that O vacancies and the stacking faults caused an abnormality in the metal−O bond vibration for nanobelts and nanosheets and led to red-shifting in phonon frequencies.[68] In the present case, a similar structure might exist in the substoichiometric $MoO_{3-\delta}$ nanocrystals, which would result in the red-shifting of the band in UV absorption. It is not clear which types of defects will lead to a blue-shift in vibrational frequencies. In addition, different regions in the nanobelts contain different defects which would imply that different shifts in the UV−vis spectra should be observed. However, this does not seem to be the case and replaces the overall blue-shifting or red-shifting phenomena. Therefore, alternative models that are used to describe the different band-shifting patterns are needed. Moreover, more hydroxyl groups adsorbed onto the surfaces of MoO_3 nanocrystals, which was verified by the former results of FT-IR analysis. The modified surfaces of the MoO_3 nanobelts might lead to the formation of a surface state energy band, which caused the adsorption at longer wavelengths. Under this condition, blue-shifting in the UV absorption may be counteracted by the red-shifting due to the dielectric confinement effect. As a result, the band gap energy of nanobelts decreases compared to that of polycrystalline and prism-like particles.

Conclusion

Uniform MoO_3 nanobelts and prism-like particles have been successfully fabricated by using a one-step and facile hydrothermal procedure. Our results indicate that the morphology of one-dimensional MoO_3 nanostructures can be controlled with the addition of common nitrates. The possible growth mechanism of molybdenum trioxide prism-like particles is proposed. We believe that the one-dimensional growth of $MoO_3 \cdot 2H_2O$ with monoclinic structure will lead to the formation of linear Mo−O−Mo in orthorhombic molybdenum trioxide. BET specific surface areas of the as-prepared molybdenum trioxide nanobelts and nanoprisms are 67−79 $m^2\ g^{-1}$. The band gap energies of these MoO_3 nanomaterials are shape-dependent (prism-like particles > nanobelts), and significant blue-shifting and red-shifting phenomena were observed for prism-like particles and nanobelts, respectively. These phenomena may be attributed to the internal strains model, defects, and dielectric confinement effects. The simple morphology controllable synthesis of nanoparticles holds promise for applications in electrochromic and photochromic devices.

Acknowledgment. We gratefully acknowledge the financial support from NSFC 20331030 and NSFC 20471058. We also appreciate Ms. M. Y. Li and Mr. L. H. Ge for the help in the FE-SEM and TEM measurements.

Supporting Information Available: The SEM micrographs of annealed MoO_3 nanobelts and prism-like particles (Figure S1), and the nitrogen adsorption isotherms for as-prepared and annealed MoO_3 nanobelts and prism-like structure (Figure S2). This material is available free of charge via the Internet at http://pubs.acs.org.

References and Notes

(1) Tito, T.; Paul, O.; Nigel, L. P. *Chem. Mater.* **2001**, *13*, 3843.

(2) Tanda, S.; Tsuneta, T.; Okajima, Y.; Inagaki, K.; Yamaya, K.; Hatakenaka, N. *Nature* **2003**, *42*, 972.
(3) Iijima, S. *Nature* **1991**, *354*, 56.
(4) Tenne, R.; Margulis, L.; Genut, M.; Hodes, G. *Nature* **1992**, *360*, 444.
(5) Rao, C. N. R.; Govindaraj, A. G.; Deepak, F. L.; Gunari, N. A.; Nath, M. *Appl. Phys. Lett.* **2001**, *78*, 1853.
(6) Dloczik, L.; Engelhardt, R.; Ernst, K.; Fiechter, S.; Seiber, I.; Könenkamp, R. *Appl. Phys. Lett.* **2001**, *78*, 3687.
(7) Yada, M.; Mihara, M.; Mouri, S.; Kuroki, M.; Kijima, T. *Adv. Mater.* **2002**, *14*, 309.
(8) Wu, J.; Liu, S.; Wu, C.; Chen, K.; Chen, L. *Appl. Phys. Lett.* **2002**, *81*, 1312.
(9) Manna, L.; Scher, E. C.; Alivisatos, A. P. *J. Am. Chem. Soc.* **2000**, *122*, 12700.
(10) Zhang, Y.; Zhu, J.; Zhang, Q.; Yan, Y.; Wang, N.; Zhang, X. *Chem. Phys. Lett.* **2000**, *317*, 504.
(11) Yang, P. D.; Lieber, C. M. *J. Mater. Res.* **1997**, *12*, 2981.
(12) Dai, H. J.; Wong, E. W.; Lu, Y. Z.; Fan, S. S.; Lieber, C. M. *Nature* **1995**, *375*, 769.
(13) Dai, Z. R.; Gole, J. L.; Stout, J. D.; Wang, Z. L. *J. Phys. Chem. B* **2002**, *106*, 1274.
(14) Wang, Z. L.; Gao, R. P.; Pan, Z. W.; Dai, Z. R. *Adv. Eng. Mater.* **2001**, *3*, 657.
(15) Pan, Z. W.; Dai, Z. R.; Ma, C.; Wang, Z. L. *J. Am. Chem. Soc.* **2002**, *124*, 1817.
(16) Trentler, T. J.; Hickman, K. M.; Goel, S. C.; Viano, A. M.; Gibbons, P. C.; Buhro, W. E. *Science* **1995**, *270*, 1791.
(17) Duan, X. F.; Lieber, C. M. *Adv. Mater.* **2000**, *12*, 298.
(18) Morales, A. M.; Lieber, C. M. *Science* **1998**, *279*, 208.
(19) Pan, Z. W.; Dai, Z. R.; Wang, Z. L. *Science* **2001**, *291*, 1947.
(20) Peng, X. S.; Zhang, L. D.; Meng, G. W.; Wang, X. F.; Wang, Y. W.; Wang, C. Z.; Wu, G. S. *J. Phys. Chem. B* **2002**, *106*, 11163.
(21) Ma, R. Z.; Bando, Y.; Zhang, L. Q.; Sasaki, T. *Adv. Mater.* **2004**, *16*, 918.
(22) Dai, Z. R.; Pan, Z. W.; Wang, Z. L. *J. Phys. Chem. B* **2002**, *106*, 902.
(23) Gundiah, G.; Govindaraj, A.; Rao, C. N. R. *Chem. Phys. Lett.* **2002**, *351*, 189.
(24) Pan, Z. W.; Dai, Z. R.; Wang, Z. L. *Appl. Phys. Lett.* **2001**, *80*, 309.
(25) Zhang, J.; Zhang, L. *Solid State Commun.* **2002**, *122*, 493.
(26) Yao, J. N.; Hashimoto, K.; Fujishima, A. *Nature* (*London*) **1992**, *355*, 624.
(27) Yang, Y. A.; Cao, Y. W.; Loo, B. H.; Yao, J. N. *J. Phys. Chem. B* **1998**, *102*, 9392.
(28) Comini, E.; Faglia, G.; Sberveglieri, G.; Cantalini, C.; Passacantando, M.; Santucci, S.; Li, Y.; Wlodarski, W.; Qu, W. *Sens. Actuators, B* **2000**, *68*, 168.
(29) Reddy, K. R.; Ramesh, K.; Seela, K. K.; Rao, V. V.; Chary, K. V. R. *Catal. Commun.* **2003**, *4*, 112.
(30) Liu, H.-F.; Liu, R.-S.; Liew, K. Y.; Johnson, R. E.; Lunsford, J. H. *J. Am. Chem. Soc.* **1984**, *106*, 4117.
(31) Zhang, W.; Oyama, S. T. *J. Phys. Chem.* **1996**, *100*, 10759.
(32) Li, X. L.; Li, Y. D. *Chem. Eur. J.* **2003**, *9*, 2726.
(33) Tenne, R.; Margulis, L.; Genut, M.; Hodes, G. *Nature* **1992**, *360*, 444.
(34) Hagrman, P. J.; Hagrman, D.; Zubieta, J. *Angew. Chem., Int. Ed.* **1999**, *38*, 2638.
(35) Hershfinkel, M.; Gheber, L. A.; Volterra, V.; Hutchison, J. L.; Margulis, L.; Tenne, R. *J. Am. Chem. Soc.* **1994**, *116*, 1914.
(36) Zach, M. P.; Ng, K. H.; Penner, R. M. *Science* **2000**, *290*, 2120.
(37) Satishkumar, B. C.; Govindaraj, A.; Nath, M.; Rao, C. N. R. *J. Mater. Chem.* **2000**, *10*, 2115.
(38) Lou, X. W.; Zeng, H. C. *Chem. Mater.* **2002**, *14*, 4781.
(39) Li, Y. B.; Bando, Y. *Chem. Phys. Lett.* **2002**, *364*, 484.
(40) Liu, T.; Xie, Y.; Chui, B. *Langmuir* **2000**, *16*, 9015.
(41) Antonelli, D. M.; Trudeau, M. *Angew. Chem., Int. Ed.* **1999**, *38*, 1471.
(42) Li, Y. B.; Bando, Y.; Golberg, D.; Kurashima, K. *Appl. Phys. Lett.* **2002**, *81*, 5048.
(43) Li, X. L.; Liu, J. F.; Li, Y. D. *Appl. Phys. Lett.* **2002**, *81*, 4832.
(44) Patzke, G. R.; Michailovski, A.; Krumeich, F.; Nesper, R.; Grunwaldt, J.-D.; Baiker, A. *Chem. Mater.* **2004**, *16*, 1126.
(45) Rietveld, H. M. *J. Appl. Crystallogr.* **1969**, *2*, 65.
(46) Zhang, Y. W.; Si, R.; Liao, C. S.; Yan, C. H. *J. Phys. Chem. B* **2003**, *107*, 10159.
(47) Ho, C.; Yu, J. C.; Kwong, T.; Mak, A. C.; Lai, S. *Chem. Mater.* **2005**, *17*, 4514.
(48) Krebs, B. *Acta. Crystallogr.* **1972**, *B28*, 2222.
(49) Böschen, I.; Krebs, B. *Acta Crystallogr.* **1974**, *B30*, 1795.
(50) Wang, X.; Li, Y. D. *Angew. Chem., Int. Ed.* **2002**, *41*, 4790.
(51) Fang, Y. P.; Xu, A. W.; You, L. P.; Song, R. Q.; Yu, J. C.; Zhang, H. X.; Li, Q.; Liu, H. Q. *Adv. Funct. Mater.* **2003**, *13*, 955.
(52) Zhang, D. F.; Sun, L. D.; Yin, J. L.; Yan, C. H. *Adv. Mater.* **2003**, *15*, 1022.
(53) Pacholski, C.; Kornowski, A.; Weller, H. *Angew. Chem., Int. Ed.* **2002**, *41*, 1188.
(54) Penn, R. L.; Banfield, J. F. *Science* **1998**, *281*, 969.
(55) Epifani, M.; Imperatori, P.; Mirenghi, L.; Schioppa, M.; Siciliano, P. *Chem. Mater.* **2004**, *16*, 5495.
(56) Guzmann, G.; Yebka, B.; Livage, J.; Julien, C. *Solid State Ionics* **1996**, *86*−*88*, 407.
(57) Dong, W.; Dunn, B. *J. Mater. Chem.* **1998**, *8*, 665.
(58) Nazri, G. A.; Julien, C. *Solid State Ionics* **1992**, *53*−*56*, 376.
(59) Neeraj, S.; Kijima, N.; Cheetham, A. K. *Chem. Phys. Lett.* **2004**, *387*, 2.
(60) Van Leeuwen, R. A.; Huang, C.-J.; Kammler, D. R.; Switzer, J. A. *J. Phys. Chem.* **1995**, *99*, 15247.
(61) Sian, T. S.; Reddy, G. B. *Sol. Energy Mater. Sol. Cells* **2004**, *82*, 375.
(62) Alivisatos, A. P. *J. Phys. Chem.* **1996**, *100*, 13226.
(63) Ekimov, A. I.; Efros, Al. L.; Onushchenko, A. A. *Solid State Commun.* **1985**, *56*, 921.
(64) Efros, Al. L.; Rosen, M. *Annu. Rev. Mater. Sci.* **2000**, *30*, 475.
(65) Ffros, Al. L.; Efros, A. L. *Sov. Phys. Semicond.* **1982**, *16*, 772.
(66) Zhang, S.-L.; Zhu, B.-F.; Huang, F.; Yan, Y.; Shang, E.; Fan, S.; Han, W. *Solid State Commun.* **1999**, *111*, 647.
(67) Gao, Y. H.; Bando, Y.; Sato, T. *Appl. Phys. Lett.* **2002**, *81*, 2267.
(68) Dai, L.; Chen, X. L.; Zhang, X. N.; Lin, A. Z.; Zhou, T.; Hu, B. Q.; Zhang, Z. *J. Appl. Phys.* **2002**, *92*, 1062.